

Sigma and hydrodynamic modes along the critical line

H. Fujii^a and M. Ohtani^{b,y}^aInstitute of Physics, University of Tokyo, Tokyo 153-8902, Japan^bRadiation Laboratory, RIKEN, Saitama 351-0198, Japan

(February 8, 2020)

Assuming a tricritical point of the two-flavor QCD in the space of temperature, baryon number chemical potential and quark mass, we study the change of the associated soft mode along the critical line within the Ginzburg-Landau approach and the Nambu-Jona-Lasinio model. The ordering density along the chiral critical line is the scalar density whereas a linear combination of the scalar, baryon number and energy densities becomes the proper ordering density along the critical line with finite quark masses. It is shown that the critical eigenmode shifts from the sigma-like fluctuation of the scalar density to a hydrodynamic mode at the tricritical point, where we have two ordering densities, the scalar density and a linear combination of the baryon number and energy densities. We argue that appearance of the critical eigenmode with hydrodynamic character is a logical consequence of divergent susceptibilities of the conserved densities.

12.38.-t, 24.85.+p, 05.70.-a, 64.70.-p

I. INTRODUCTION

At high temperature and/or baryon density, the system governed by QCD will show a transition from an ordinary hadronic phase to a chirally symmetric, deconfined plasma phase [1,2]. The main objective of the heavy-ion programs at RHIC and at future LHC is to create this long-sought plasma state and to study collective properties of this many-body assembly [3]. These two phases would have to be separated by a boundary with singularity if chiral symmetry or confinement of QCD were exact symmetry. In reality, dynamical quarks with finite masses $m \neq 0$ make both symmetries only approximate, and their order parameters, the quark condensate and the Polyakov loop, have nonvanishing values everywhere in the phase diagram. Thus the plasma state may be smoothly connected with the ordinary hadronic state, even though they would possess qualitatively different properties from each other.

Recently a strong possibility of a critical point in the real QCD phase diagram was suggested [4{6], based on model calculations [7{10] as well as lattice QCD results [11{13]. It is the endpoint of the first order line, inferred from the crossover behavior along the temperature (T) axis and the first order transition along the axis of the baryon number chemical potential (μ_B), and is a genuine singular point with the same criticality as the Z_2 Ising model. Its location, which is sensitive to the strange quark mass m_s , is expected to be within the reach of current experimental facilities. Observable implications of this Z_2 critical point (Z_2 CP)¹ in heavy ion experiments have been discussed in the literature [4,5,14{18] such as large fluctuations of the low momentum particle distributions, and the limitations on them due to the finite space-time geometry of collision events. This Z_2 CP will become a critical cornerstone in the QCD phase diagram once its location is confirmed in experiments.

Based on the approximate chiral symmetry, the scalar density is usually taken as the order parameter of the Ginzburg-Landau (GL) effective potential to describe the critical behavior at the Z_2 CP. In this description all the singularities associated with the Z_2 CP seemingly originate from softening of the scalar density fluctuations as the effective potential becomes flat there. Especially, it might be concluded that the sigma meson becomes massless as an immediate consequence of this critical point.

As a basic fact, however, we should strictly distinguish between the chiral critical point with $m = 0$ and the Z_2 CP with $m \neq 0$ even within the chiral effective models. When the chiral symmetry is exact, the $T - \mu_B$ plane is divided into two domains of the symmetric and broken phases with a boundary line. But the symmetry argument is unable to fix the order of the singularity of this line, especially the possible existence of the tricritical point (TCP) on this line. Since the Z_2 CP at finite quark mass is the remnant of this TCP, the relation of the Z_2 CP to the chiral symmetry

Em ail: hfujii@phys.s.u-tokyo.ac.jp

^yEm ail: ohtani@rarfexp.riken.jp

¹In the QCD thermodynamics this point is referred to as critical end point (CEP). In this paper we use Z_2 CP instead of CEP, to indicate the symmetry of the point.

is very obscure. In fact, Z_2 is not the symmetry of the underlying interactions, but of the thermodynamic potential at this particular isolated point in the $T\{\mu_B\}$ phase diagram [19]. From this point of view the Z_2 CP is different from the chiral critical point.

The attractive potential indicates the large fluctuation of the scalar density. At the chiral critical point, this is related to softening of the sigma meson mode, so as to form a symmetric excitation spectrum together with the pions. On the other hand, there is no such symmetry constraint at the Z_2 CP. Actually the scalar fluctuation linearly mixes with fluctuations of baryon number density and energy density, and therefore not only the sigma mode but also the hydrodynamic mode are to be taken into account there to study the associated soft mode. Consequently the fate of the sigma meson mode at the Z_2 CP is non-trivial.

Recent calculations of the dynamic mode in the scalar channel using the chiral models [16,20] indeed show that the sigma meson is massive at the Z_2 CP. Furthermore, another scalar mode with space-like momentum dispersion is identified as the soft mode associated with the Z_2 CP in the Nambu–Jona-Lasinio (NJL) model [20]. In this paper we shall confirm the result of Ref. [20] on the more general ground using the time-dependent Ginzburg–Landau (TDGL) approach, and extend the study to discuss the changeover of the soft modes along the critical line in the $T\{\mu_B\}$ space within the TDGL approach as well as the NJL model.

Our investigation is based on two fundamental observations about the Z_2 CP. The first point is that the proper ordering density at the Z_2 CP is a linear combination of the scalar, baryon number and internal energy densities [19,21], as mentioned above. Because of this mixing all the susceptibilities of these densities diverge at the Z_2 CP with the same critical exponent. In contrast, in the chiral critical transition, the susceptibility of the scalar density diverges with exponent of the $O(4)$ model in the two-flavor case, while the other susceptibilities of the baryon number and the energy have the smaller exponent.

The second is a consequence on the dynamics following from the conservation of the baryon number and the energy. The fluctuations of these conserved densities² are intrinsically soft and constitute the hydrodynamic modes, whose excitation energies vanish as the wavevector q goes to zero. Susceptibilities of these conserved densities in turn have the spectral contributions solely from these hydrodynamic modes when expressed as a sum of mode spectra [22,24]. Hence the divergence of the susceptibility of a conserved density must be accompanied by critical slowing of a hydrodynamic mode. The spectral contribution from this hydrodynamic mode may well be involved in the scalar susceptibility through the mixing at the Z_2 CP.

At an $O(4)$ critical point ($O(4)$ CP) the importance of the hydrodynamic mode depends on which phase we start from. The hydrodynamic mode plays no critical role in the symmetric phase whereas the scalar condensate makes the mixing possible in the broken phase. The situation becomes more subtle at the TCP, where the $O(4)$ critical line shifts to the first-order line. Only the scalar susceptibility diverges due to the softening of the sigma meson at the TCP if it is approached from the symmetric phase. Otherwise, the hydrodynamic soft mode causes the divergence in the susceptibilities of the baryon number and energy as well as the scalar one.

This paper is organized as follows. In the next section we briefly review generic properties of the phase diagram of QCD with two flavors near the TCP using the GLE effective potential. It is stressed that at the TCP there are two relevant order parameters, the scalar condensate and a conserved density which is a linear combination of the baryon number and entropy densities. Then we include the dynamics using the TDGL model. Writing the susceptibilities as a spectral sum, we discuss the relative weight of the spectral contributions from the sigma and hydrodynamic modes. It is pointed out that the hydrodynamic contribution generates the discontinuity of the baryon number and entropy susceptibilities at the $O(4)$ CP, and that this hydrodynamic mode gives the divergence at the TCP approached from the broken phase and also at the Z_2 CP. In XIII we perform the same analysis using the NJL model as an illustration. The GLE effective potential with two ordering densities are numerically constructed there. The directions at the critical points are shown and discussed in relation to the divergences of the susceptibilities. The spectral origins of these divergences are studied with the relative weight of the mode spectra, and in detail based on the poles and residues of the scalar response function. Sections IV and V are devoted to discussions and summary. In Appendix A we prove the relation between the susceptibility and the response function, and in Appendix B we present the explicit formulas of the response functions in the NJL model. The results with the chiral quark model is briefly reported in Appendix C.

²Momentum density is neglected here for simplicity.

II. GENERIC ANALYSIS

A. Structure of the phase diagram and order parameters

Let us briefly review the phase structure near the TCP [25,5,15]. It is known that the critical properties near the TCP are described, up to logarithmic corrections, with the Ginzburg-Landau effective potential

$$\begin{aligned} Z &= \phi_0(T; B) + \int d^3x \left[a(T; B)^2 + b(T; B)^4 + c(T; B)^6 \right] h \\ Z &= \phi_0(T; B) + \int d^3x f(T; B; h); \end{aligned} \quad (1)$$

where $f(\phi)$ denotes the (non-)singular part of the effective potential, and $c > 0$. The pseudo-scalar density is set to zero and neglected here in the mean field approximation. The critical exponents can be easily found from (1) at the mean field level. Along the line of the first order transition within the symmetry plane ($h = 0$), we have

$$f = a^2 + b^4 + c^6 - c^2 \left(\frac{2}{1} \right)^2; \quad (2)$$

where three minima with $\phi = 0$; $\phi_1(T; B)$ coexist (dashed line in Fig. 1). The baryon number and entropy densities are functions of ϕ^2 due to symmetry, and discontinuous across the boundary between the symmetric phase ($\phi = 0$) and the broken phase ($\phi = \phi_1$). At the TCP, where $a = b = 0$, these three phases coalesce and the first order line ($b = -2\sqrt{ac}$) smoothly joins with the O(4) critical line ($a = 0; b > 0$).

Once a small explicit breaking field h is exerted, the O(4) critical line disappears and the TCP is lifted to the Z_2 CP. The line of Z_2 CP as a function of h is determined by the condition, $f^0 = f^{\text{odd}} = f^{\text{even}} = 0$ ($\phi = \phi_1$), which is solved for a negative b with $a = 3b^2/5c$, $b = -\sqrt{5}h$ and $\phi = \text{sign}(h)(h/16)^{1/5}$. Two lines of Z_2 CP with $h \neq 0$ form the edge of the wing-like surface of the first order transition in the $a(b, h)$ space, and these lines connect smoothly to the O(4) critical line at the TCP. This wing structure is mapped into the physical phase space of T , B and h (see Fig. 1).

The slope of the first order boundary can be related to the discontinuities of the densities across the boundary via the Clapeyron-Clausius relation [10],

$$\frac{dT}{dB} = -\frac{B}{s}; \quad \frac{dT}{dh} = -\frac{1}{s}; \quad \frac{dh}{dB} = -\frac{B}{s} \quad (3)$$

with baryon number density B and entropy density s . The chiral broken phases with $\phi = \phi_1$ coexist within the symmetry plane $h = 0$, and accordingly there is no gap in B and s across this symmetry plane. Only the scalar density bifurcates as the ordering density at the O(4)CP approached from the symmetric phase. Its correlations with the "energy-like" densities vanish $h \rightarrow 0$ because of the symmetry in ϕ in the symmetric phase.

From the relation (3) we know that all of T , B and s generally have discontinuities across the wing because there is no reason for any of these slopes to vanish once $h \neq 0$. Let us discuss the energy-like and ordering densities around the Z_2 CP. First we introduce the "temperature-like" field as a vector tangential to the coexistence boundary. Then the energy-like density is defined as the thermodynamic variable conjugate to this temperature-like field. This density has no discontinuity in the vicinity of the critical point. Since the boundary is two-dimensional, there are two independent temperature-like fields and correspondingly two energy-like densities. Next the ordering density is defined as the density whose correlations with the energy-like densities vanish at the critical point approached from the "symmetric" phase along the temperature-like direction. The conjugate field of this ordering density is no longer tangential to the coexistence boundary. There is a single ordering density at the Z_2 CP, which is in general a linear combination of T , B and s . Since all the susceptibilities of these densities include the same singular fluctuation, they diverge at the Z_2 CP with the same critical exponent.

The coexistence wing is squeezed to be one-dimensional at the TCP, where two lines of the Z_2 CP and the line of the first order transition with $h = 0$ merge and smoothly connect to the single O(4) critical line. Thus at the TCP we have only one energy-like density, which will be a linear combination of B and s . Accordingly there are two ordering densities from dimensionality. The obvious one is the scalar density related to the chiral symmetry and the other is another linear combination of B and s representing the Z_2 symmetry of the potential at this particular point. It is sometimes useful to construct the effective potential with two ordering densities, ϕ and ϕ' , which become soft at the TCP.

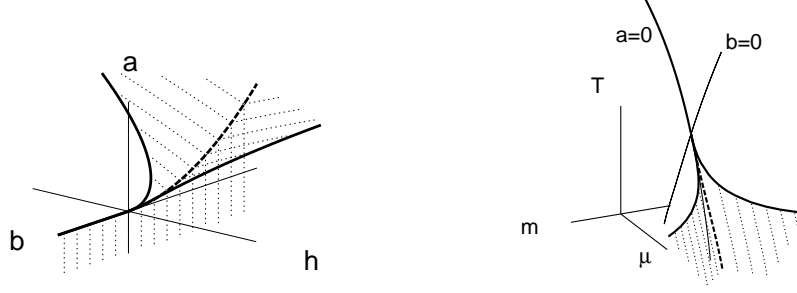


FIG. 1. Schematic phase diagram around the TCP in the $a\{b\{h$ space and the physical $T\{\{m$ space. The three critical lines are shown in bold lines which meet at the origin (TCP). The curve of three-phase coexistence is drawn in a bold dashed line which ends at TCP. The two-phase coexistence surface are hatched by thin dotted lines. The mapping into a physical phase space is shown in the right figure (NJL model result).

The same observation can be made by looking at the susceptibilities directly. There are three fields h , a and b in the effective potential (1). The singular parts of the corresponding susceptibilities form a 3-by-3 matrix ($i, j = h, a, b$),

$$\chi_{ij} = \begin{pmatrix} 0 & 1 & 2 & 4 & 3 & 1 \\ \partial & 2 & 4 & 2 & 8 & 4 \\ 4 & 3 & 8 & 4 & 16 & 6 \end{pmatrix} A \quad (4)$$

with χ_h the scalar susceptibility,

$$\chi_h = \frac{1}{V} \frac{\partial^2}{\partial^2 h} = \frac{1}{2a + 12b^2 + 30c^4}; \quad (5)$$

where χ_h takes the value at the extremum of the potential. When the $O(4)$ CP is approached from the symmetric phase, $\chi_{aa} = \chi_{bb} = 0$. In the broken phase the situation is different. The singular part of (1) gives a finite contribution $\chi_{aa} = 1/(3b)$ as the $O(4)$ CP is approached with $b^2 = a/2b \neq 0$, although the divergent susceptibility is still the scalar one alone. The singular contribution to χ_{aa} eventually blows up at the TCP approached along the $O(4)$ critical line. In fact, the TCP may be understood as a usual critical point with the ordering density ϕ conjugate to a , sitting on the chiral phase boundary. When the TCP is approached from the broken phase with $b = h = 0$, the scalar ordering density vanishes slowly $\phi^4 = a/3c$, and χ_h and χ_{aa} diverge like $1/\phi^2$ and $1/\phi^4$, respectively, while χ_b is still non-singular. Note that the divergence of χ_{aa} at the TCP indicates the infinities in the baryon number and energy³ susceptibilities, or equivalently the isothermal compressibility and specific heat, respectively.

All these susceptibilities in (4) diverge at the Z_2 CP, where $\phi \neq 0$. With the finite condensate we can diagonalize this matrix of the susceptibilities, leaving only one singular susceptibility. The resulting eigenvalues are $(0, 0, (1 + 4^2 + 16^6)\chi_h)$, with eigenvectors $^t(2; 1; 0)$, $^t(4^3; 0; 1)$, $^t(1; 2; 4^3)$, respectively. For small ϕ or h , we see that the ordering density is approximately a linear combination of the densities ϕ and ϕ' .

The fluctuations of these two ordering densities, ϕ and ϕ' become large near the TCP as explained above, and should be included as the soft degrees of freedom, especially when we discuss the dynamic aspects. We generalize the free energy so as to have two ordering densities,

$$\mathcal{Z} = \int d^3x \left[a_0 \phi^2 + b_0 \phi^4 + c \phi^6 + \frac{1}{2} \phi'^2 + \frac{1}{2} \chi_h \phi \phi' + \phi_0 \right] \quad (6)$$

³The fluctuation of the energy density is a linear combination of those of the baryon number and entropy densities. In this paper we sometimes use the energy susceptibility and entropy susceptibility interchangeably.

Coupling between ϕ and ϕ' must respect the underlying chiral symmetry and the simplest coupling is $\phi^2 \phi'$. A flat direction of this potential appears at a critical point in the $\{\phi, \phi'\}$ plane. In the case of the $O(4)CP/TCP$ it is in the direction reflecting the symmetry while the direction will become a linear combination of the two densities at the Z_2CP . Eliminating the density ϕ' by $\phi = \phi' = \phi^2 + \phi' - \phi^2 = 0$, we recover the original form of the free energy with $a = a_0 + \phi^2$ and $b = b_0 - \frac{1}{2} \phi^2$, up to an analytic term.

B. Dynamics

We may introduce the dynamics to the system described by the free energy (6) phenomenologically [26]. We have seen in the previous subsection that there are two ordering densities conjugate to the fields, h and a at the TCP, and that a linear combination of these two densities will become the relevant ordering density at the Z_2CP for small h or a . We should include at least these two densities in order to describe the soft dynamics. Furthermore, it is known that (non-linear) mode-mode coupling between the fluctuations of the ordering densities and other (non-critical) hydrodynamic modes are important in general to describe the dynamics in the critical region [26], which is beyond the scope of this work [27]. We will see, however, that the coupled system of the two ordering densities in the mean field approximation yields already a non-trivial result.

1. Mixing between scalar and conserved densities

Deviation of the densities from the absolute equilibrium gives rise to time evolution of the system. Here we assume simple phenomenological equations of motion for densities ϕ and ϕ' as

$$L(\partial_t \phi) = -\gamma; \quad L'(\partial_t \phi') = -\gamma'; \quad (7)$$

where $L(\partial_t \phi)$ and $L'(\partial_t \phi')$ are the differential operators. Appropriate forms of L and L' are unknown in this description. But as a strong constraint we know that the operator L' must be consistent with the conservation of the density ϕ' and describe the hydrodynamic motion. As a typical hydrodynamic evolution, we consider here the diffusion motion $L'(\partial_t \phi') = \partial_t^2 \phi' = q^2 \phi'$ with wavevector q . Note that the diffusion is time-irreversible. We assume propagating motion $L(\partial_t \phi) = \partial_t^2 \phi = q^2 \phi$ for the scalar density, identifying this mode as the sigma meson which degenerates with the propagating pions at the $O(4)CP/TCP$. Other possible forms are considered below in this section. The transport coefficients $\gamma, \gamma' > 0$ are treated as constants here.

For small deviations $\phi = \phi_0 + \tilde{\phi}$ and $\phi' = \phi'_0 + \tilde{\phi}'$ from the equilibrium values, we linearize these equations of motion with respect to $\tilde{\phi}$ and $\tilde{\phi}'$ to obtain

$$L(\partial_t \tilde{\phi}) + \gamma \tilde{\phi} = 0; \quad L'(\partial_t \tilde{\phi}') + \gamma' \tilde{\phi}' = 0; \quad (8)$$

where $\gamma = \frac{1}{2} \chi_h = \frac{1}{2} \chi_d$, etc. The soft eigenmodes of the system is determined by the condition

$$\frac{1}{2} \chi_h + \left(\frac{1}{2} \chi_h + \frac{4}{q^2} \right) \frac{1}{i\omega + q^2} = 0; \quad (9)$$

where χ_h is the scalar susceptibility given in (5), and we introduced a $(\omega)^2$ term in χ_h with coefficient $\frac{1}{2}$. The eigenmodes for small q are found as $\omega = \omega_0; \omega_d$ with

$$\frac{\omega_0^2}{2} = \left(\frac{1}{2} \chi_h + \frac{4}{q^2} \right) \left(\frac{1}{2} + \frac{4}{\chi_h + \frac{4}{q^2}} \right) q^2; \quad \frac{\omega_d}{q^2} = \frac{\frac{1}{2} \chi_h}{\chi_h + \frac{4}{q^2}} \frac{1}{q^2}; \quad (10)$$

where χ_j is the susceptibility of the density ϕ' .

The eigenmode ω_0 is oscillating while ω_d has the diffusion-like hydrodynamic character. The ω_0 vanishes at the $O(4)CP$, being the critical eigenmode. Although the hydrodynamic mode ω_d is an intrinsic soft mode of the system, it does not show the critical slowing there. When the TCP is approached from the symmetric phase, the situation is

the same. On the other hand, at the TCP approached from the broken phase, both frequencies slow down, reflecting the divergence of the susceptibilities, which seems reflecting the existence of two independent ordering densities there.

At the Z_2 CP the susceptibilities χ_h and χ_j diverge with the same exponent due to the linear mixing. The propagating ω_o is a fast mode there due to the non-zero condensate $\phi = (\hbar/16)^{1/5}$, whereas the hydrodynamic slow mode $\omega_d = q^2 = \omega_j^2$ becomes the critical mode ($\omega_j^2 \rightarrow 0$) associated with the Z_2 CP. This result is similar to the level-crossing phenomenon where the mode coupling makes the lower energy mode lowered further. The explicit q^2 factor of ω_d stemming from the hydrodynamic character results in the larger dynamic critical exponent $z = 4$ in the mean field level, which makes ω_d apparently slower than the ω_o mode. In contrast, at the $O(4)$ CP, the linear mixing is banned by the underlying chiral symmetry.

2. Susceptibility as a spectral sum

Inverse of the differential operator (9) with the retarded boundary condition is the response function

$$(\chi; q) = \frac{q^2}{((\omega + i\eta)^2 + \omega_o^2)(-\omega + i\eta + \omega_d^2)} = \frac{\frac{-i\eta}{q^2} + 1}{2} \frac{2}{-\omega^2 + \omega_h^2 + 4\omega^2 + q^2}; \quad (11)$$

which characterizes the time-dependent response of these densities to the external fields, h and j , within the linear approximation. The susceptibility is obtained in the limit of ($\eta \rightarrow 0; q \rightarrow 0$). The response function is analytic in the upper complex ω plane, which fact allows us to express generally the susceptibility as a sum of the mode spectra:

$$(\chi; q) = \frac{1}{i} \sum_l \frac{d\omega_l}{\omega_l} \text{Im}(\chi; q); \quad (12)$$

where a ultraviolet regularization is understood if necessary. This expression shows that the divergence at a critical point should come from an infrared enhancement of the spectral function because the spectral function itself is usually integrable.

Using this expression we can examine the relative weight of each mode contribution to the susceptibility. In our case, the oscillating and diffusion modes give spectral contributions as

$$\chi_h = \lim_{q \rightarrow 0} \frac{1}{i} \sum_l \frac{d\omega_l}{\omega_l} \text{Im}(\chi; q) = \chi_h \frac{\omega_h^2}{\omega_h^2 + 4q^2} + \frac{4q^2}{\omega_h^2 + 4q^2}; \quad (13)$$

and

$$\chi_j = \lim_{q \rightarrow 0} \frac{1}{i} \sum_l \frac{d\omega_l}{\omega_l} \text{Im}(\chi; q) = \chi_j (0 + 1); \quad (14)$$

Here the first term in the bracket originates from the poles ω_o and the second from ω_d .

First, we note that only the diffusion-like ω_d pole contributes to the susceptibility of j . This is a robust result following from the conservation of the density j . Existence of the current j such that $\partial_t j + \nabla \cdot j = 0$ dictates that the frequencies of the modes contributing to the j susceptibility must vanish as q goes to zero. We can formally show that the spectrum of the j response function behaves as $\lim_{q \rightarrow 0} \text{Im}(\chi_j; q) = \omega_d^2 / \omega_h^2$ (see Appendix A). Conversely, we can state that softening of the hydrodynamic mode must accompany the divergence of χ_j .

Second, the ratio of the ω_d spectral contribution to the total in the scalar susceptibility,

$$R = \frac{4q^2}{\omega_h^2 + 4q^2} = \frac{\omega_d^2}{\omega_h^2}; \quad (15)$$

goes to unity at the TCP approached from the broken phase and at the Z_2 CP, which means that the leading divergence of the scalar susceptibility is also generated by the ω_d spectrum at these critical points. Even at the $O(4)$ CP approached from the broken phase the ω_d spectrum gives a finite portion of the divergence $0 < R < 1$ since $\omega_h^2 \neq 0$. This result can be understood by rewriting the scalar response function as

$$\chi_h(\omega; q) = \chi_h^{(0)}(\omega; q) \frac{1}{1 - \frac{\chi_j^{(0)}(\omega; q)}{\chi_h^{(0)}(\omega; q)}}; \quad (16)$$

where $\chi_h^{(0)}(\omega; q) = 1/(L(\omega + i0) + \dots)$ and $\chi_j^{(0)}(\omega; q) = 1/(L(\omega) + \dots)$. The denominator expresses the linear mixing between the "bare" \sim and \sim modes through the coupling \dots . Even though the coupling becomes smaller as the $O(4)$ CP is approached from the broken phase, softening of the mediating "bare" \sim propagator provides $1/\omega^2$ factor, which results in the finite mixing of the ω_d mode in the scalar channel. This is a simple example indicating the importance of the mode coupling near the critical point.

In summary, the \sim and \sim fluctuations mix and form two kinds of eigenmodes, ω_o and ω_d . We find that along the $O(4)$ critical line approached from the broken phase, the critical eigenmode shifts from the sigma meson like ω_o to the diffusion like ω_d mode at the TCP. In contrast, when we approach the TCP from the symmetric phase, the scalar susceptibility χ_h is given completely by the critical ω_o spectrum without any mixing of the \sim fluctuation. At the Z_2 CP the ω_o mode becomes a fast mode while the whole divergence comes from the critical softening of the ω_d spectrum with the hydrodynamic character.

3. Cases with other types of motion

In more microscopic NJL model calculation in the later section, the mode with the hydrodynamic character is provided as the mode of Landau-damping type, contrary to the macroscopic analysis in the previous subsection, and we may change the time evolution operator accordingly as $L(\omega) = -i\omega = -i\sqrt{q^2}$. More generally, the sigma mode may be oscillating or relaxing ($L(\omega) = -\omega^2 = -i\omega$ or $-i\omega$) while the possible hydrodynamic fluctuation can be the diffusion, Landau-damping type, or sound motion ($L(\omega) = -i\omega = -q^2$; $-i\omega = -\sqrt{q^2}$, or $-\omega^2 = -q^2$). Generally, coupling with other hydrodynamic modes are basically important to describe the correct dynamic behavior of the system [26,27]. We stress here that our result on the critical eigenmodes at the critical points are independent on these ambiguities. The only important fact is that the operator L has the hydrodynamic character, and therefore intrinsically soft mode of the system. In any of these choices, we find the eigenmodes for small q^2 as

$$L(\omega) = (-\omega^2 + 4q^2); \quad L(\omega) = -i\omega; \quad (17)$$

Note that the typical mode frequencies of the diffusion, Landau-damping type and sound-like dispersions vanish $\omega \rightarrow 0$ as $q \rightarrow 0$, and satisfy the spectral property following from the conservation law

$$-\frac{1}{2\pi} \text{Im} \frac{1}{L(\omega) + i0} \delta(\omega) \quad \text{as } q \rightarrow 0; \quad (18)$$

Finally we note that these hydrodynamic modes drop out in the limit of the response function:

$$\chi^{(0)}(\omega; 0) = \lim_{\omega \rightarrow 0} \frac{1}{\omega} \frac{d}{d\omega} \text{Im} \chi^{(0)}(\omega; 0) = \lim_{\omega \rightarrow 0} \frac{1}{\omega} \frac{d}{d\omega} \omega^0 \delta(\omega) = 0; \quad (19)$$

III. Nambu-Jona-Lasinio Model with Tricritical Point

As an definite illustration, we shall study the spectral contributions of the collective modes at critical points in the NJL model, and confirm that the result is consistent with the TDGL approach. We remark here that, unlike in the TDGL approach, there are no bare bosonic modes, but the collective eigenmodes are dynamically generated through the interaction between the quarks and their softening causes the divergences at the critical points.

A. Effective potential and susceptibilities

We analyze the simplest version of the NJL model [28,23,29] $L = q(\bar{\psi}\psi) + g[(q\bar{q})^2 + (q\bar{q}_5 - \bar{q}_5 q)^2]$; in the mean field approximation ($\langle q\bar{q} \rangle = \text{const}$, $\langle q\bar{q}_5 - \bar{q}_5 q \rangle = 0$). The thermodynamics is described by the effective potential,

$$(T; \mu; \bar{\psi}\psi) = V = \int \frac{d^3k}{(2\pi)^3} E + T \ln(1 + n_+) + T \ln(1 - n_-) + \frac{1}{4g} (2g)^2; \quad (20)$$

where $n_{\pm} = (e^{(E \mp \mu)/T} + 1)^{-1}$, $E = \sqrt{M^2 + k^2}$, $M = m - 2g$, and $\mu = 2N_f N_c = 2 \times 2 \times 3 = 12$ with N_f and N_c the numbers of flavor and color, respectively. Here μ is the quark chemical potential. The true thermodynamic state is

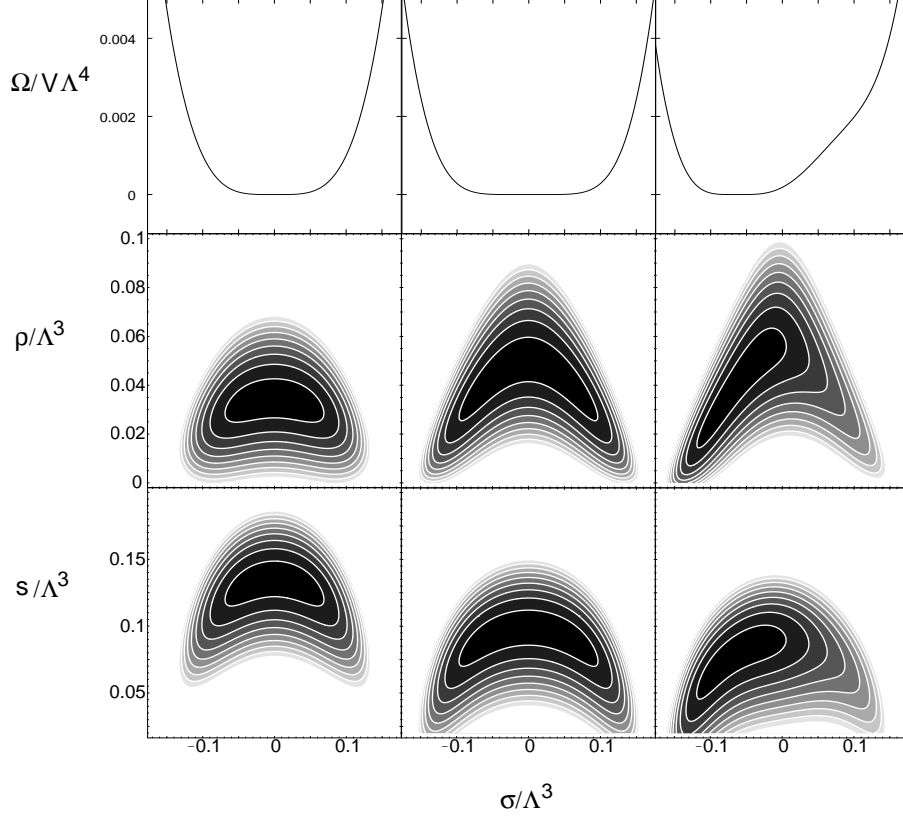


FIG. 2. Effective potentials as functions of σ , ρ and s at three critical points, $O(4)CP$, TCP and Z_2CP .

determined by the extremum condition, $\partial\Omega/\partial\sigma = 0$, and the corresponding grand potential is $\Omega(T; \sigma; m)$. We define the model with the three-momentum cutoff and with the coupling constant $g^2 = 2.5$ which allows the TCP . In the following, all the dimensionful quantities are expressed in the units of Λ .

Expansion of the effective potential around $\sigma = 0$ with $m = 0$ gives rise to

$$\begin{aligned} \Omega(T; \sigma; 0) = V &= \int \frac{d^3k}{(2\pi)^3} [k^2 - T \ln(1 - n_+^0) - T \ln(1 - n_-^0)] + \frac{1}{2} \left(\frac{1}{2g} \right)^2 J^0 (2g)^2 + \frac{1}{2} \frac{I^0}{4} (2g)^4 + \\ &= \Omega(T; \sigma; 0) = V + a(T; \sigma) (2g)^2 + b(T; \sigma) (2g)^4 + \dots \end{aligned} \quad (21)$$

where the suffix 0 indicates the quantity evaluated in the massless limit. The first term is the non-singular part of the free energy in the GL description. The integrals I^0 and J^0 are given in Appendix B. The TCP determined by $a = b = 0$ appears at $T_c = 0.20362$ and $\sigma_c = 0.49558$.

As explained in xII, it is useful to introduce the effective potential with another relevant ordering density besides the σ in studying the behavior of the quark number susceptibility and specific heat near the TCP and the Z_2CP . From the physical grand potential $\Omega(T; \sigma; m)$, we can construct the Landau effective potential with two ordering densities σ and s in the following way: first we introduce the free energy $F(T; \sigma; s)$ via

$$F(T; \sigma; s) = V = \Omega(T; \sigma; m) = V + \dots \quad (22)$$

where $\sigma = \sigma(T; \sigma; s)$ and $m = m(T; \sigma; s)$ are defined by inverting the functions

$$\sigma = \frac{1}{V} \frac{\partial \Omega}{\partial \sigma}(T; \sigma; m); \quad m = \frac{1}{V} \frac{\partial \Omega}{\partial m}(T; \sigma; m): \quad (23)$$

Then introducing new parameters $\tilde{\sigma}$ and \tilde{m} , we define the Landau-type effective potential as

$$\tilde{\Omega}(T; \tilde{\sigma}; \tilde{m}; \tilde{s}) = V = F(T; \sigma; s) = V + \dots = \Omega(T; \sigma; m) = V + \dots \quad (24)$$

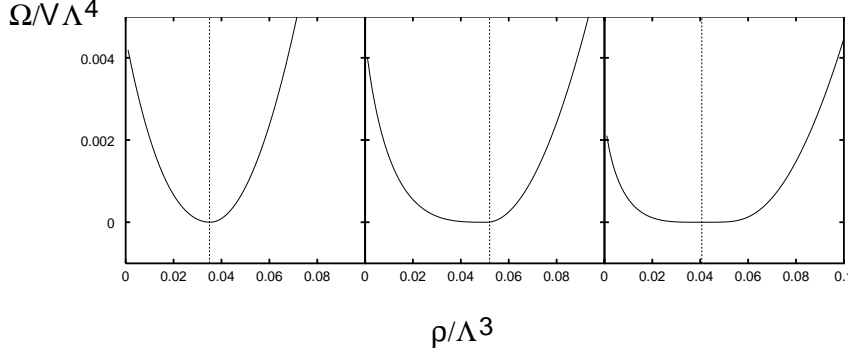


FIG. 3. Effective potentials as functions of p/Λ^3 at three critical points, a chiral transition, the TCP and the Z_2 CP.

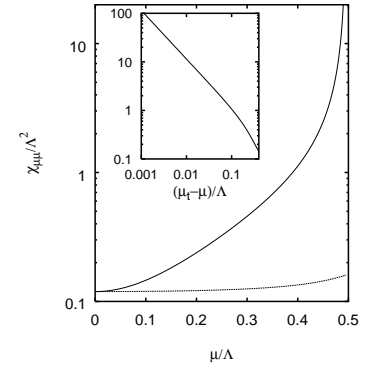


FIG. 4. The χ_{qq}/Λ^2 along the $O(4)$ critical line approached from the broken phase. The value from the symmetric phase is shown in a dashed line. Inset: The χ_{qq}/Λ^2 (solid) as a function of $(\mu_t - \mu)/\Lambda$.

The extremum condition for the densities μ and s yields $\mu = \mu_c$ and $m = m_c$, recovering the physical grand potential $\Omega(T; \mu_c, m_c)$. Use of the entropy density s instead of the quark number μ is straightforward. It is known that the effective potential constructed in this way must be convex and cannot be defined in the mixed phase. Fortunately in the NJL model we can bypass this difficulty by supplementing the unphysical grand potential $\Omega(T; \mu, m)$ defined with the unstable solutions of the gap equation, which corresponds to the non-convex part of the potential $\tilde{\Omega}$.

One can easily show that the susceptibilities $\chi_{ij} = \frac{1}{V} \partial^2 \Omega / \partial \mu_i \partial \mu_j$ ($i, j = T, \mu, m$) are equal to the inverse of the curvature matrix of the GL effective potential at the extremum point. From this fact the divergence of the susceptibilities at a critical point is related to the appearance of a particular flat direction in the GL effective potential.

In Fig. 2 we show the effective potential with two ordering densities at three critical points, $O(4)$ CP with $(T; \mu) = (0.3419; 0.3)$, TCP, and Z_2 CP with $(T; \mu, m) = (0.1498; 0.5701; 0.01)$ in the units of Λ . The critical instability at these points is usually discussed using the effective potential (20) with a single variable μ based on chiral symmetry, which is shown in the upper panels. The flat curvature of this potential means the divergence of the scalar susceptibility. At the $O(4)$ CP it is clear from the potential with two ordering densities (μ, s) , or (μ, m) , that the μ axis is indeed the symmetry direction of the system. The densities μ and s depend on μ^2 when calculated from (20) with $m = 0$. This fact is seen here as a quadratic bending of the potential valley. Thus the fluctuation of these densities are weaker than that of μ , and the susceptibilities of the quark number and the entropy has the smaller exponent β .

At the Z_2 CP, on the other hand, the flat direction of the GL potential is not parallel to the μ axis in the $\{\mu, s\}$ and $\{\mu, m\}$ planes. The proper flat direction is a linear combination of the three densities of μ , s , and m , and all the susceptibilities of them diverge with the same exponent at the Z_2 CP.

It will be very instructive to introduce the GL function with single ordering density by eliminating μ by $\mu \sim \mu_c = 0$ in favor of s , as shown in Fig. 3. The curvature at the extremum coincides with the inverse of the quark number susceptibility. In case of the $O(4)$ CP (left panel) the curvature does not vanish, implying the finite susceptibility χ_{qq} . It takes different values depending on from which side we approach the equilibrium value of μ . Since the μ^2 and μ^4 terms of the potential (21) disappear at the TCP (middle panel in Fig. 2) and μ changes with μ^2 along the potential valley, the quadratic term of the μ potential in Fig. 3 vanishes on the side corresponding to the broken phase, which indicates a critical point for μ . On the higher density side, in contrast, the curvature is nonvanishing. Since the potential is essentially the same as the potential (20), we may equally well choose s or m as an ordering density rather than μ to describe the criticality at Z_2 CP.

Along the line of the $O(4)$ critical line we show the quark number susceptibility χ_{qq} as a function of μ in Fig. 4. The χ_{qq} is discontinuous across the critical line, and the limiting value from the broken phase grows toward the TCP and eventually diverges there as is described with the GL potential ($\mu \rightarrow 1=b$) [15]. The χ_{TT} also behaves in the same way, except that at the point $\mu = 0$ the χ_{TT} has no gap because no linear coupling with μ is allowed due to the symmetry under $\mu \rightarrow -\mu$.

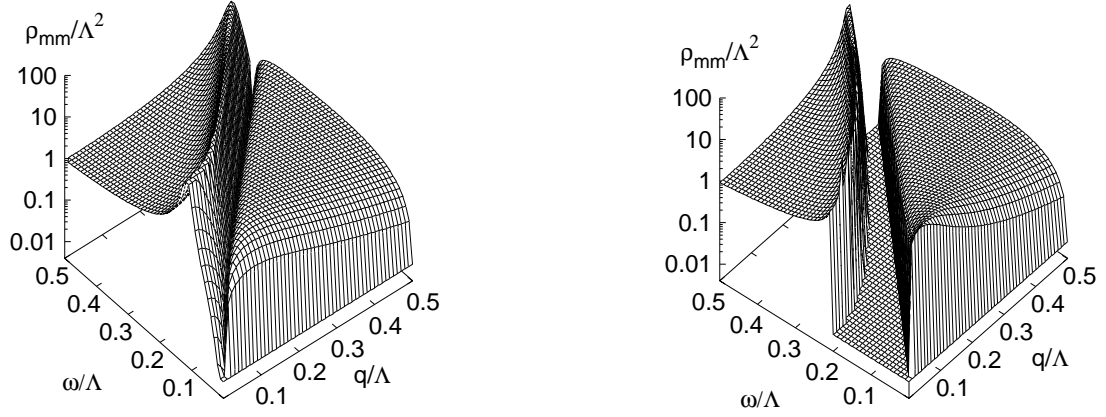


FIG. 5. Spectral functions of the scalar channel above (Left, $T = 0.35$) and below (Right, $T = 0.339$) the chiral transition point with $\mu = 0.3$ in the (q, ω) plane.

B. Response functions and mode spectra

The spectral origin of the critical divergence can be investigated by studying the spectral function which is obtained as the imaginary part of the response function. We discuss here the structure of the collective eigenmode, which couples with the relevant susceptibilities and shows softening at the critical point.

The response functions in the NJL model are calculated as [30]

$$\chi_{ab}(iq_4; q) = \chi_{ab}^{(0)}(iq_4; q) + \chi_{am}^{(0)}(iq_4; q) \frac{1}{1 - 2g_{mm}(iq_4; q)} 2g_{mb}(iq_4; q); \quad (a; b = \sigma; m; \pi); \quad (25)$$

Here the polarizations are defined with the imaginary time quark propagator $S(K) = 1/(K + M)$ as

$$\chi_{ab}(iq_4; q) = \frac{1}{(2\pi)^3} \int d^3k \text{Tr}_n \text{tr}_{\text{color}} S(K) S(K - q) \chi_{ab}^{(0)}; \quad (26)$$

where $q_4 = 2\pi T(1/2 - Z)$, $K = (k; k_4 + i)$, χ is an appropriate Dirac matrix, and the traces are taken over the flavor, color and Dirac indices. $\chi = 1$ for the scalar, $i\gamma_4$ for the baryon number, and H_{MF} for χ with

$$H_{MF} = i\frac{1}{2} \text{Tr} \{ \gamma_4 + M + i\gamma_4 \}; \quad (27)$$

We calculate here the response function with H_{MF} the energy operator in the mean field approximation instead of the entropy, because the entropy has no microscopic expression as it is defined only in equilibrium. The real time response function is obtained from the imaginary time propagator through the usual replacement $iq_4 \rightarrow q_4 + i$ in the final expression. The static response function in the long wavelength limit reduces to the corresponding susceptibility, $\lim_{q \rightarrow 0} \chi_{ab}(0; q) = \chi_{ab}$. Especially, $\chi_{\sigma\sigma} = T^2 \chi_{\sigma\sigma}$.

The one-loop polarization $\chi_{ab}^{(0)}(q; q)$ are the response functions of the free quark gas with mass M , and contain no contributions from the collective mode. In our simple NJL model, the collective mode is generated by the bubble sum encoded in the denominator of Eq. (24) and there are two kinds of collective motions [20]: the sigma meson mode and the particle(hole) (p(h)) mode. In Ref. [20] it is argued that the soft mode associated with the Z_2 CP is not the sigma meson but the p(h) motion.

The spectral function $\rho_{mm}(q; q)$ of the scalar response function [31] yields

$$\begin{aligned} \rho_{mm}(q; q) &= 2\text{Im} \chi_{mm}(q; q) = 2\text{Im} \frac{1}{1 - 2g_{mm}(q; q)} \\ &= \frac{2\text{Im} \chi_{mm}(q; q)}{[1 - 2g_{mm}(q; q)]^2 + [2g_{mm}(q; q)]^2}; \end{aligned} \quad (28)$$

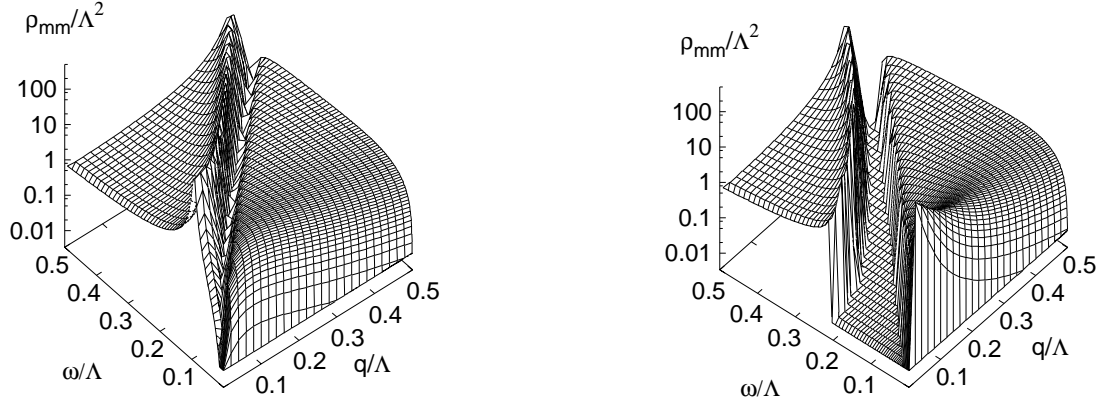


FIG. 6. Spectral functions of the scalar channel above (Left, $T = 0.210$) and below (Right, $T = 0.2035$) TCP in the ω - q plane.

We notice that the spectrum $2\text{Im } \chi_{mm}(\omega; q)$ of the free quark gas is enhanced by the bubble-type correlation in the denominator.

The scalar spectral functions are shown at $T = 0.350$ and 0.339 near the $O(4)$ CP with $(T_c; \mu_c) = (0.3419, 0.3)$ in Fig. 5. One should keep in mind that the $\chi_{mm}(\omega; 0)$ spectrum of the sigma meson at $q = 0$ in the broken phase is hard to be seen in this figure. The sigma meson spectrum is softening just above and below the $O(4)$ CP (see also xIIID). Besides the sigma spectrum we clearly find the p-h mode spectrum in the space-like momentum region, whose strength looks stronger in the broken phase. As we approach the TCP, as is shown in Fig. 6, this p-h mode spectrum grows in the small q region in the broken phase, while in the symmetric phase it does not show such an enhancement.

We show in Fig. 7 the spectral functions of the scalar channel as well as the vector channel (quark number response) at the Z_2 CP with $m = 0.01$. In the scalar channel clearly seen are the two spectral peaks of the sigma meson and the p-h motion in medium, respectively [20]. This spectral structure is to be compared with that of the free quark case given in Appendix B. The most significant feature in χ_{mm} is the critical enhancement in the $\omega \rightarrow 0$ region provided by the p-h mode, which gives rise to the divergence of the scalar susceptibility. Although the sigma meson shows the clear spectral peak in this model, the mode is massive due to the explicit symmetry breaking by the current quark mass.

The spectral function of the quark number susceptibility, $\chi(\omega; q)$, also contains these two spectral contributions, but the sigma spectrum strongly diminishes as $q \rightarrow 0$. It is worthwhile to note the fact that $\chi_{mm}(\omega > 0; 0) = 0$ and $\text{Im } \chi_{mm}(\omega; 0) / \omega \rightarrow 0$ as $q \rightarrow 0$, which reflects the conservation of the quark number. Thus the response function

$\chi(\omega; q)$ obtained in (25) in the random phase approximation (RPA), too, shares the same property, and the sigma meson cannot couple to the quark number susceptibility at $q = 0$. Therefore the divergence of χ at Z_2 CP must come solely from the softening of the p-h spectrum. The same is true for T_T .

C. Spectral sum along the critical line

In the previous subsection we have identified the soft mode associated with Z_2 CP as the p-h motion [20] generated in the scalar channel whereas at the $O(4)$ CP the sigma meson mode becomes soft. Let us examine how the changeover of the soft mode from the sigma meson to the p-h one occurs along the critical line. Once we noticed that the difference between the two limits, $\chi_{mm}(0^+; 0)$ and $\chi_{mm}(0; 0^+)$, is caused by the hydrodynamic mode spectrum $\chi(\omega; 0)$ as $q \rightarrow 0$, it is easy to calculate the ratio of the spectral strength of the two types of spectral contributions. In these limits the explicit form of the RPA scalar response functions in the broken phase (with $m = 0$) yields, respectively,

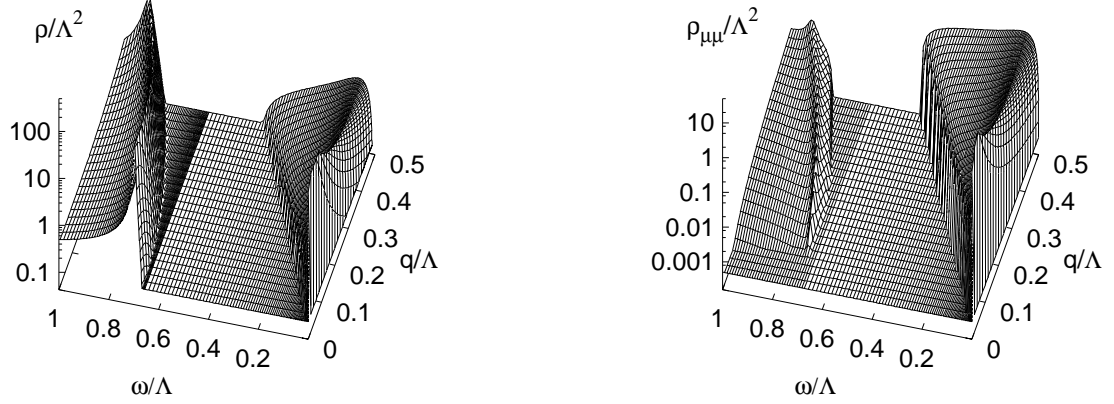


FIG. 7. Spectral functions of the scalar and the quark number susceptibilities at the Z_2 CP with $m = 0.01$.

$$\begin{aligned} \chi_{mm}(0^+;0) &= \frac{1}{2g} \frac{1}{2g - 4M^2 I(0^+;0)} \quad 1; \\ \chi_{mm}(0;0^+) &= \frac{1}{2g} \frac{1}{2g - 4M^2 I(0;0^+)} \quad 1; \end{aligned} \quad (29)$$

where function $I(\omega; q)$ is given in Appendix B. Then we can define the ratio R of the hydrodynamic spectrum to the total strength of the scalar susceptibility in the NJL model as

$$R = \frac{\chi_{mm}(0;0^+) - \chi_{mm}(0^+;0)}{\chi_{mm}(0;0^+)} = \frac{I(0^+;0) - I(0;0^+)}{I(0^+;0)}; \quad (30)$$

On the other hand, these limits in the symmetric phase result in the same value

$$\chi_{mm}(0;0) = \frac{1}{2g} \frac{1}{1 - \frac{1}{2g} \frac{1}{g}} \quad 1; \quad (31)$$

which means no hydrodynamic contribution to the scalar susceptibility there ($R = 0$). The ρ h mode must be decoupled from χ_{mm} if we approach the chiral critical line from the symmetric phase. Meanwhile we know that the corresponding ratios for the susceptibilities of the conserved quantities are always unity ($R = 1$), which can be explicitly seen with the expressions given in Appendix B.

The ratio R (30) is shown in Fig. 8 as a function of ω along the critical line. We find that even in the $O(4)$ chiral transition at zero baryon number density ($\mu = 0$) the hydrodynamic spectrum contributes to the divergence by a finite fraction. This contribution of the hydrodynamic spectrum increases toward the TCP, and eventually saturates the divergence at the TCP, where $I(0;0^+) = I^0 = 0$ but $I(0^+;0) \neq 0$. This behavior is completely in parallel with the TDGL approach.

The fact that the ρ h mode gives a finite fraction of the divergence at the $O(4)$ CP might be again unexpected from the viewpoint of the sigma meson as the associated soft mode there. Indeed, the sigma meson spectrum generates the total divergence when the critical point is approached from the symmetric phase. We should note here that the mixing of the scalar fluctuation in the broken phase is the origin of the discontinuity of the baryon number and energy susceptibilities across the boundary and that only the scalar ρ h mode with the hydrodynamic character can couple with the fluctuations of these conserved quantities. Since the transitions between the scalar and other channels is proportional to M , the ρ h spectral strength in the scalar is necessarily of order $1/M^2$ so as to bring a finite contribution to χ_{mm} and χ_{TT} .

We note that the scalar ρ h motion of the NJL model is possible only in medium, but always possible in medium even in the symmetric phase, where the ρ h contribution should be decoupled from the scalar susceptibility. One may ask the reason for the decoupling of the ρ h spectrum. The absorption amplitude of the collective ρ h mode with momentum q by a left-handed quark $q_L(k)$ is proportional to a spinor product $u_R(k+q)u_L(k)$. In the symmetric

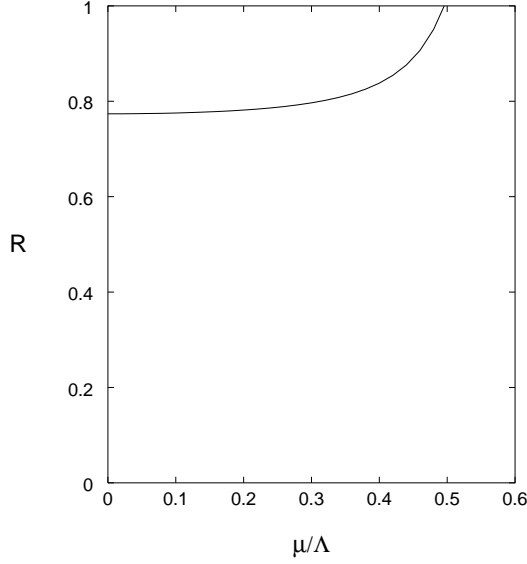


FIG. 8. Ratio (30) of the spectral contribution along the chiral critical line approached from the broken phase. $R \rightarrow 1$ toward TCP.

phase this coupling must contain a helicity flip because chirality and helicity are identical for a massless quark, and vanishes in the $q \rightarrow 0$ limit. It is easy to show that $u_R(k+q)u_L(k) \propto \mathbf{j} \cdot \mathbf{q}$. For a massive quark in the broken phase, each of the left- and right-handed states has both helicity components, and thus $u_R(k+q)u_L(k) \propto 2M \neq 0$ in the $q \rightarrow 0$ limit.

D. Behavior of poles and residues

Let us discuss a little more details of the spectral contributions to the susceptibility, studying the poles and the residues of the scalar response function

$$\chi_{mm}(\mathbf{l}; \mathbf{q}) = \frac{1}{2g} \frac{1}{1 - 2gJ(\mathbf{q}) + 2g(4M^2 - \mathbf{q}^2)I(\mathbf{l}; \mathbf{q})} \quad (32)$$

near the NJL critical points. It is useful to represent the spectral contributions as

$$\chi_{mm}^{\text{pole}}(\mathbf{l}; \mathbf{q}) = \sum_{i=\sigma, \text{ph}} \frac{R_i(\mathbf{q})}{\mathbf{l} + \mathbf{l}_i(\mathbf{q})} \quad (33)$$

with the poles corresponding to the sigma meson (σ) near $2M$ and the p(h) mode on the negative imaginary axis [20]. We would obtain the susceptibility as $q \rightarrow 0$ after setting $\mathbf{l} = 0$. As for the p(h) contribution, however, we take into account the kinematic condition $|\mathbf{j}| = qj < 1$ for the spectrum via

$$\frac{1}{2} \sum_{\mathbf{j}} \frac{d!}{\mathbf{j}!} 2\text{Im} \frac{R_{\text{ph}}(\mathbf{q})}{\mathbf{l} + \mathbf{l}_{\text{ph}}(\mathbf{q})} = \frac{R_{\text{ph}}}{\mathbf{l}_{\text{ph}}} \frac{2}{\mathbf{j}!} \tan^{-1} \frac{\mathbf{j} \cdot \mathbf{j}}{\mathbf{j}!_{\text{ph}} \mathbf{j}} \quad (34)$$

The scalar susceptibility in this approximation is expressed as a sum of the sigma and p(h) pole contributions:

$$\chi_{mm}^{\text{pole}}(0; 0^+) = 2 \frac{R}{\mathbf{l}} + \lim_{q \rightarrow 0} \frac{R_{\text{ph}}}{\mathbf{l}_{\text{ph}}} \frac{2}{\mathbf{j}!} \tan^{-1} \frac{\mathbf{j} \cdot \mathbf{j}}{\mathbf{j}!_{\text{ph}} \mathbf{j}} \quad (35)$$

In Fig. 9 we show numerical results of the poles and residues of the scalar response function (32) as functions of $t = jT - T_c jT_c$ with fixed $\mu = \mu_c$. The behavior of them can be understood as follows:

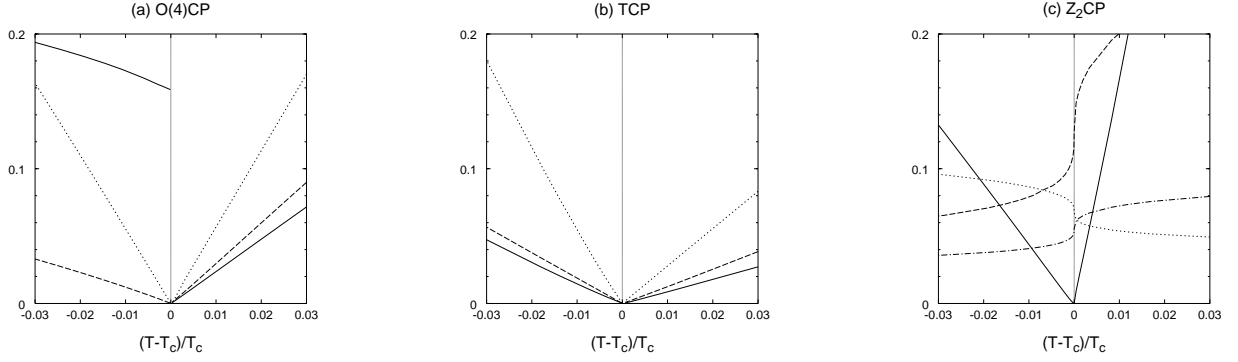


FIG. 9. Scaling of the pole positions and the residues near the critical points. (a) O(4)CP: The solid line denotes $j_{ph} = j$ for $t < 0$ and $j_{ph}^3 = j$ for $t > 0$ with $q = 0.01$. The residue $R_{ph} j^2$ for $t < 0$ and $R_{ph} j^{2=3}$ for $t > 0$ is shown in a dashed line. The sigma pole $j^2 = 4M^2$ with $q = 0$ for $t < 0$ and $(\text{Re } j)^2$ for $t > 0$ in a dotted line. (b) TCP: The similar plot to the O(4) case, but $(j_{ph} = j)^2$ and j^4 for $t < 0$. (c) Z₂CP: $(j_{ph} = j)^{3=2} 10$, $R_{ph} j$ and $\text{Re } j$ are shown in solid, dashed and dotted lines, respectively. The $R_R j$ is also drawn in a dash-dotted line.

Across the O(4)CP In the broken phase ($1 - 2gJ(0) = 0$), the sigma pole with $q = 0$ locates at $j = 2M$ on the real axis, whose residue is $R = (M - I(2M; 0))$. These quantities scale as $1 = R = M = \frac{1}{m_m} \frac{t^{1=2}}{q} \frac{t^{1=2}}{q}$. In the symmetric phase ($M = 0$), $\frac{1}{m_m} \frac{1}{q} \frac{1}{2gJ(0)} t$. The complex sigma meson pole appears at $j = \frac{1}{m_m} I(j; 0) t^{1=2}$ with the residue $1 = \frac{1}{m_m} I(j; 0) t^{1=2}$. In both cases, the sigma mode gives the appropriate strength of the divergence $R = \frac{1}{m_m} t^{1=2}$.

The p{h} mode arises from the j dependence of the function $I(j; q)$. Since we are interested in the behavior in the small j and q region with $u = j < 1$, we may approximate the function I as

$$I(j; q) = I(0; 0^+) + iu \text{Im } I(0)^0; \quad (36)$$

where $\text{Im } I(u)^0 = (d/du) \text{Im } I(u; j; q)|_{j=0}$. In the broken phase, the pole is fixed by the condition, $I(j; q) = 0$ as $j_{ph} = i j_{ph} I(0; 0^+)$, whose residue $R_{ph} = i j_{ph} M^2 t^{1=3} j$. Similarly in the symmetric phase the condition $1 = (2g) J(0) j^3 = j j \text{Im } I(0) = 0$ fixes the pole position as $j_{ph} = i (\frac{1}{m_m} j)^{1=3} (t j)^{1=3}$ with the residue $R_{ph} = i j j = (\frac{1}{m_m} j)^{2=3} t^{2=3} j^{j=3}$. Then according to Eq. (34) the spectral contribution is estimated to be

$$\frac{R_{ph}}{j_{ph}} \tan^{-1} \frac{j j}{j_{ph} j} = \frac{1}{t}; \quad (37)$$

$$\frac{R_{ph}}{j_{ph}} \tan^{-1} \frac{j j}{j_{ph}} = \frac{1}{t} \tan^{-1} \frac{j j^{2=3}}{t^{1=3}} \neq 0 \quad (38)$$

for the broken and symmetric cases, respectively, as $j j \neq 0$. We note that the p{h} mode gives finite portion of the divergence at the O(4)CP approached from the broken phase due to the enhancement of the residue by $1 = M^2$, despite that the frequency $j_{ph} = j j$ shows no critical slowing. The decoupling of the p{h} mode in the symmetric phase is correctly described by the behavior of the pole.

Across the TCP At the TCP, $I(0^+; 0) \neq I(0; 0^+) = I^0 = 0$. When we approach from the broken phase $\frac{1}{m_m} = (2g)^2 4M^2 I(0; 0^+) t$ while $j = M t^{1=4}$. Then the sigma mode slows down, but cannot generate the leading divergence because $R = \frac{1}{m_m} t^{1=2}$ whereas $\frac{1}{m_m} t^{1=4}$. The fact $I(0; 0^+) = t^{1=2}$ changes the scaling of the p{h} mode into $j_{ph} = t^{1=2} j j$ with the residue $t^{1=2} j j$ which gives rise to the correct order of the divergence

$$\frac{R j}{j_{ph} j} \tan^{-1} \frac{j j}{j_{ph}} = \frac{1}{t} \tan^{-1} \frac{1}{t^{1=2}} = \frac{1}{t}; \quad (39)$$

The p{h} mode must correspond to the critical eigenmode. On the other hand, if the TCP is approached from the symmetric phase, the p{h} mode is decoupled from the scalar susceptibility and the critical sigma mode generates the total divergence. It is very interesting that the soft mode associated with the TCP is different between the symmetric and broken phases.

At the Z₂CP The sigma meson mode has a finite energy gap of order $2M$ in our model. The pole position of the p{h} mode can be evaluated as $j_{ph} = i \frac{1}{m_m} j j t^{2=3} j j$ with its residue $i j j$, which gives rise to

$$\frac{\chi_{ph}}{\chi_{ph}} \tan^{-1} \frac{\chi_{ph}}{\chi_{ph}} \quad m \quad t^{-2=3} : \quad (40)$$

From this estimate, we see that the ρ mode properly accounts the divergence of the scalar susceptibility at the Z_2 CP, and therefore the softening of the ρ mode is the origin of the critical divergence at the Z_2 CP.

IV. DISCUSSIONS

In the microscopic calculation with the NJL model, we have seen that the collective ρ mode, besides the sigma meson mode, is generated in the scalar channel and brings the spectral contributions to the channels of the conserved quantities through the mixing when $M \neq 0$. This ρ spectrum makes the susceptibilities of χ and χ_{TT} discontinuous across the $O(4)$ critical line, and eventually gives rise to the critical divergences at the TCP and the Z_2 CP. This role of the ρ mode is consistent with the behavior of the hydrodynamic mode in the TDGL analysis. We remark here that this ρ mode in the NJL model is the time-reversible Landau damping type. In the phenomenological TDGL approach, on the other hand, we assumed the time-irreversible diffusion motion for the conserved density, which seems more appropriate to the non-equilibrium soft dynamics. It would be very interesting to study how a time-irreversible equation of motion emerges out of the time-reversible microscopic theory.

The flat curvature of the effective potential is usually referred to as the vanishing screening mass, which naively hints the reduction of a kind of particle mass. As we approach the $O(4)$ CP, the sigma meson mass actually gets reduced to cause the critical divergence. However, approaching the Z_2 CP, we see that the flat curvature leads to the vanishing diffusion constant of the hydrodynamic mode [20,21,27]. In general, the potential curvature expresses the stiffness of the system with respect to the variation of the ordering density. The dynamic quantity related to this stiffness can be the particle mass, sound velocity, relaxation constant or diffusion constant, depending on the equation of motion of the critical eigenmode.

In the Z_2 CP case, the linear mixing of the conserved densities in the proper ordering density dictates that the critical eigenmode should have hydrodynamic character. We have seen that the sigma (meson-like) mode is massive and is decoupled from the slow dynamics. It is explicitly argued in Ref. [27] that the remaining set of slow modes is equivalent to that of the liquid-gas critical point [20,21]. In the course of heavy ion events passing by the Z_2 CP, it is important to study the observable implications of critical slowing of hydrodynamic fluctuations in baryon number and entropy densities [5,18]. The growth of the diffusive fluctuations within the finite space-time would get renewed interest [5,14].

The critical soft mode of the TCP is different between the symmetric and broken phases. The sigma mode becomes the critical eigenmode and the hydrodynamic one behaves normally if the critical point is approached from the exactly symmetric phase. Otherwise the critical eigenmode bears the hydrodynamic character and the sigma mode slows down only moderately, which implies the importance of the hydrodynamic fluctuations near the TCP, the endpoint of the first order line sitting on the chiral phase boundary. Theoretically and also experimentally it is worthwhile to clarify and classify the dynamic critical behavior at the TCP [27].

In the QCD thermodynamics the first order transition is believed to occur at finite temperature in the massless three-flavor case [2] and in the pure gluonic case [1], where the chiral symmetry and the Z_3 center symmetry are exact, respectively. As varying masses of the quarks from these two limits, we expect the critical points (line) at the edge of the first-order region. For example, a Z_2 CP is studied in the T - μ plane at zero baryon density with three quark flavors of equal mass in lattice QCD in Ref. [19]. At a critical mass value, a particular linear combination of the quark condensate and the energy density is identified as a proper order parameter, which should be mapped to the magnetization in the Z_2 Ising model. We expect that a hydrodynamic mode related to the energy fluctuation shows critical slowing at this Z_2 CP, whose spectrum may be detected in the lattice QCD. The dynamic critical behavior of this point is also of importance. We may naively expect the same universality with the liquid-gas criticality, although it is non-trivial since there is no linear mixing of the baryon number fluctuation in the ordering density due to the symmetry $B \rightarrow B$. Furthermore, the lines and surfaces of the QCD critical points in the T - μ - μ_s space are speculated [32]. One can also extend the space to the isospin channel [33]. Generally at such a critical point the proper ordering density becomes a linear combination involving conserved densities. Since the critical eigenmode must have the hydrodynamic character in this case, the dynamic critical nature would be quite different from the case with (e.g.) the exact chiral symmetry.

Our identification of the soft modes along the critical line is done within the mean-field approximation. Fluctuations around the mean fields are known to become crucial for describing the singular behavior at the critical points correctly. To this end we should utilize mode-coupling theory or dynamic renormalization group method. The mean-field analysis provides a good starting point to identify an appropriate set of the slow modes.

V. SUMMARY

The fundamental points about the Z_2 CP are following: (1) in the absence of the chiral symmetry, the ordering density becomes a linear combination of the scalar density, the baryon number density and the energy density, in general, and their susceptibilities have the same critical exponent. In describing the static property of this critical point one may equally well take any of these densities as the ordering density. (2) Then the critical eigenmode must be the hydrodynamic one which can cause the critical divergence of the susceptibility of the conserved density. On the other hand, in the chiral transition approached from the symmetry phase, the exact chiral symmetry prohibits the linear mixing of the hydrodynamic mode in the fluctuation of the ordering density. We have showed this point using the TDGL approach as well as the microscopic NJL model.

We have studied the change of the critical eigenmode along the $O(4)$ critical line. When the critical point is approached from the symmetric phase, the soft mode is indeed the sigma meson mode. On the other hand, approaching from the broken phase we see the scalar condensate allows the linear mixing between the sigma and hydrodynamic modes, and eventually at the TCP the hydrodynamic mode turn out to be the critical eigenmode which generates the leading critical divergence. Thus the shift of the critical mode from the sigma meson to the hydrodynamic mode occurs at the TCP. And the soft mode at the TCP seems crucially depends on from which phase one is approaching the point.

The criticality of the Z_2 CP is given by the softening of a hydrodynamic mode. The sigma mode remains as a fast mode due to the explicit breaking and is decoupled from the soft dynamics. Based on this understanding, we should study fluctuations with the hydrodynamic character, such as baryon number and entropy fluctuations [5,18,34] in locating the Z_2 CP experimentally.

In the QCD thermodynamics with three quark flavors, several kinds of end points are speculated. One should keep in mind that at these points the hydrodynamic mode will become the critical eigenmode once the conserved density is linearly mixed in the ordering density. One should note that the approximate symmetry of the underlying interactions does not provide any reason for singularity in the phase diagram.

ACKNOWLEDGMENTS

The authors thank K. Ohnishi for discussions in the early stage of this work. They are very grateful to T. Matsui, M. Rho and M. A. Stephanov for fruitful discussions and comments. The important comment by T. Kunihiro on the susceptibility of the conserved density is acknowledged. H.F. thanks the warm hospitalities extended to him at YITP and at KIAS, where parts of this work were performed. This work is supported in part by the Grants-in-Aid for Scientific Research of Monaka-sho (Grant No. 13440067).

APPENDIX A: SUSCEPTIBILITY AND RESPONSE FUNCTION

The susceptibility of a (bosonic) density ρ_a in a system described with the grand potential $\Omega = -T \ln \text{tr}(\exp(-\hat{K}))$ with $\hat{K} = \hat{H} - \mu_a \int d^3x \hat{\rho}_a$ is defined as

$$\chi_{ab} = \frac{1}{V} \frac{\partial^2 \Omega}{\partial \mu_a \partial \mu_b} \quad (\text{A } 1)$$

This susceptibility is obtained as $q \rightarrow 0$ limit of the response function because

$$\begin{aligned} \chi_{ab} &= \frac{\partial}{\partial \mu_a} e^{-\frac{\Omega}{T}} \text{tr}(\hat{\rho}_b(0;0) e^{-\hat{K}}) \\ &= e^{-\frac{\Omega}{T}} \int_0^\infty ds \int d^3x \text{tr}(\hat{\rho}_b(0;0) e^{-s\hat{K}} \hat{\rho}_a(0;\mathbf{x}) e^{(1-s)\hat{K}}) \\ &= \int_0^\infty d\tau \int d^3x \chi_{ab}^{>}(\tau; \mathbf{x}) = \lim_{q \rightarrow 0} \int_0^\infty d\tau \int d^3x \langle \hat{\rho}_a(\tau; \mathbf{x}) \hat{\rho}_b(0;0) \rangle = \lim_{q \rightarrow 0} \chi_{ab}(0; \mathbf{q}) \end{aligned} \quad (\text{A } 2)$$

where we used a formula, $\frac{d}{d\mu_a} e^{-\frac{\Omega}{T}} = -\frac{1}{T} \frac{d\Omega}{d\mu_a}$ with a matrix-valued function $A(a)$, and the time dependence of the operators are defined by $\hat{\rho}_a(\tau; \mathbf{x}) = e^{\tau\hat{H}} \hat{\rho}_a(0; \mathbf{x}) e^{-\tau\hat{H}}$. The imaginary time correlation and the response function are introduced as $\chi_{ab}^{>}(\tau; \mathbf{x}) = \langle \hat{\rho}_a(\tau; \mathbf{x}) \hat{\rho}_b(0;0) \rangle$ and $\chi_{ab}(\tau; \mathbf{x}) = i \langle [\hat{\rho}_a(\tau; \mathbf{x}), \hat{\rho}_b(0;0)] \rangle$, respectively.

Once we establish the relation between the susceptibility and the response function, it is easy to express the susceptibility as an integral over the spectral density:

$$\chi_{ab} = \chi_{ab}(0; q, 0) = \lim_{q \rightarrow 0} \int_0^Z \frac{d!}{2} \frac{2\text{Im} \chi_{ab}(!; q)}{!} : \quad (\text{A } 3)$$

Specifically, when χ_a is conserved, $[\hat{K}; \hat{\chi}_a] = 0$, we can freely change the position of the operator $\hat{\chi}_a$ in the trace and the susceptibility is directly related to the equal-time correlation function S [23] via

$$\begin{aligned} \chi_{ab} &= \int_0^Z d^3x h_a(0; 0) \hat{\chi}_a(0; x) i_c \\ &= \int_0^Z d^3x S_{ab}(0; x) = \lim_{q \rightarrow 0} \int_0^Z \frac{d!}{2} S_{ab}(!; q) \\ &= \lim_{q \rightarrow 0} \int_0^Z \frac{d!}{2} \frac{2\text{Im} \chi_{ab}(!; q)}{1 - e^{-!}} : \end{aligned} \quad (\text{A } 4)$$

In the last equality we used the fluctuation-dissipation (FD) theorem, which relates the fluctuation S to the dissipative part Im of the response function. Noting the spectral condition, $\text{sign}(!) \text{Im}(!; q) \geq 0$, we conclude that these two expressions for the susceptibility coincide if and only if $\lim_{q \rightarrow 0} \text{Im}(!; q) = (!)!$. Physically this is a consequence of the existence of the current j_a such that $\partial_t \chi_a + r_a j = 0$.

APPENDIX B: EXPLICIT EXPRESSIONS

1. response functions

We present the explicit formulas and procedures to evaluate for the one-loop polarization functions.

First working in the imaginary time formalism [30], we derive the expressions for the polarization functions with make use of the frequency sum formulas:

$$\begin{aligned} I(i!_1) &= T \sum_n \frac{1}{K_E^2 + M^2} \frac{1}{(K - q)_E^2 + M^2} \\ &= \frac{1}{4E_1 E_2} \frac{1}{i!_1} \frac{n_{+1}}{E_1} \frac{n_{+2}}{E_2} \frac{n_{-1}}{i!_1 + E_1} \frac{n_{-2}}{E_2} + \frac{n_{+1}}{i!_1} \frac{n_{+2}}{E_1 + E_2} \frac{1}{i!_1 + E_1 + E_2} : \end{aligned} \quad (\text{B } 1)$$

$$\begin{aligned} I_!(i!_1) &= T \sum_n \frac{i(2K_4 - q_4)}{K_E^2 + M^2} \frac{1}{(K - q)_E^2 + M^2} \\ &= \frac{1}{4E_2} \frac{1}{i!_1} \frac{n_{+1}}{E_1} \frac{n_{+2}}{E_2} + \frac{n_{-1}}{i!_1 + E_1} \frac{n_{-2}}{E_2} + \frac{n_{+1}}{i!_1} \frac{n_{+2}}{E_1 + E_2} + \frac{1}{i!_1 + E_1 + E_2} \\ &\quad + \frac{1}{4E_1} \frac{1}{i!_1} \frac{n_{+1}}{E_1} \frac{n_{+2}}{E_2} \frac{n_{-1}}{i!_1 + E_1} \frac{n_{-2}}{E_2} \frac{n_{+1}}{i!_1} \frac{n_{+2}}{E_1 + E_2} + \frac{1}{i!_1 + E_1 + E_2} \end{aligned} \quad (\text{B } 2)$$

where $!_1 = 2!_1 T$ is the bosonic Matsubara frequency, $K = (k; !_n + i)$ the quark momentum with $!_n = (2n + 1) T$, $K_E^2 = k^2 + K_4^2$, $E_1 = \sqrt{M^2 + k^2}$, $E_2 = \sqrt{M^2 + (k - q)^2}$, and $n_{\pm 1, 2} = n(E_{1, 2})$. The q and k dependences are implicit through these quantities. Then the analytic continuation to the real frequency is done by the replacement $i!_1 \rightarrow q_0 + i$, which uniquely gives the retarded functions with the asymptotic behavior $\sim 1/q_0$ as $q_0 \rightarrow 0$.

Since the retarded function is analytic in the upper half plane, we can reconstruct it from the imaginary part using the dispersion integral,

$$\chi_{ab}(!; q) = \frac{1}{\pi} \int_0^Z \frac{d!}{!} \frac{\text{Im} \chi_{ab}(!^0; q)}{! - !^0} : \quad (\text{B } 3)$$

This relation is quite useful when we evaluate the polarization functions with finite q because the imaginary part is easier to calculate. The imaginary part comes from two physical processes in our model: the $q\bar{q}$ creation/annihilation and the mode-absorption/emission by a quark q or an anti-quark \bar{q} as shown in Fig. 10. Kinetically the former occurs for the timelike momentum with $q^2 = q_0^2 - q^2 > 4M^2$ while the latter is possible for $q^2 < 0$. Then the complex

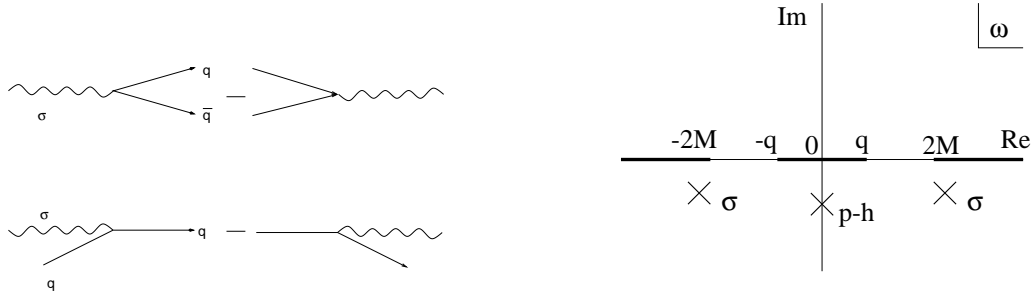


FIG. 10. Physical processes contributing to the spectrum with the detailed balance (left), and schematic cut structure of the response function (right). The meson pole and the p-h pole in the unphysical Riemann sheet are shown.

! plane has two kinds of cuts in the case of finite q . Analytic continuation of the retarded function to the lower half plane ($\text{Im } z < 0$) across one of these cuts is defined by

$$(z; q) = \frac{1}{2\pi i} \int_{-\infty}^{\infty} d\omega \frac{\text{Im}(\omega; q)}{\omega - z} + 2\text{Im}^{\text{tim/sp}}(z; q); \quad (\text{B } 4)$$

where $\text{Im}^{\text{tim/sp}}(z; q)$ is the imaginary part in the time-like or the space-like region, depending on across which cut the function is continued. Substituting these expressions to Eq. (25), we can obtain the response functions with finite q and search the poles in the unphysical Riemann sheet (see Fig. 9 cut).

The one-loop polarization function in the scalar channel yields

$$\Pi_{\text{m m}}(q_0; q) = \int \frac{d^3k}{(2\pi)^3} \frac{1}{E_1} \frac{n_{+1} n_{-1}}{E_1} + \int \frac{d^3k}{(2\pi)^3} (q^2 - 4M^2) I(q_0 + i\epsilon); \quad (\text{B } 5)$$

$$J(q_0^2) + (q^2 - 4M^2) I(q_0 + i\epsilon; q);$$

where we have shifted the momentum as $k \rightarrow k + q/2$ and $E_{1,2} = \sqrt{M^2 + (k \pm q/2)^2}$, and then introduce the cutoff at $k_{\text{max}}^2 = \frac{q_0^2}{2} - q^2/4$ for this new k . In the second line we defined the functions J and I , whose massless limits appear in the expansion series of the NJL effective potential in terms of q , Eq.(21). The integral I^0 is seemingly divergent logarithmically in the infrared region, but is actually finite because $1/n_+^0 - 1/n_-^0 \rightarrow 0$ as $k \rightarrow 0$.

After performing the angular integration using the delta function imposed by the on-shell condition, the imaginary part of the scalar polarization for $q_0 > 0$ yields

$$\text{Im} \Pi_{\text{m m}}(q_0; q) = \frac{1}{16} \int \frac{dk}{2\pi} \frac{q_0^2 - 4M^2}{E^2 - q^2/4} D(q_0; q^2); \quad (\text{B } 6)$$

$$D(q_0; q^2) = \frac{2}{n_{+1} n_{+2} + n_{-1} n_{-2}} \frac{n_{+1} n_{-1}}{E_1} \frac{n_{+2} n_{-2}}{E_2}; \quad \begin{cases} 4M^2 < q^2 < 4(M^2 + k_{\text{max}}^2) \\ q^2 < 0 \end{cases} \quad (\text{B } 7)$$

where $q^2 = q_0^2 - q^2$ and $E_P^2 = M^2 + k^2$. Due to the on-shell condition of the imaginary part, the quark energies in n are set to be $E_{1,2} = \frac{q_0}{2} \sqrt{E^2 - q^2/4}$ for $q^2 > 4M^2$ and $E_{1,2} = \frac{q_0}{2} \sqrt{E^2 - q^2/4}$ for $q^2 < 0$. The last k integration can be done analytically. The imaginary part for $q_0 < 0$ is obtained by $\text{Im}(\Pi(q_0; q)) = \text{Im}(\Pi(q_0; q))$.

Similarly, other polarization functions and their imaginary parts for $q_0 > 0$ are found and given below:

$$\Pi(q_0; q) = \int \frac{d^3k}{(2\pi)^3} \frac{1}{E_1} \frac{n_{+1} n_{-1}}{E_1} + \int \frac{d^3k}{(2\pi)^3} (q_0^2 - 4E^2) I(q_0); \quad (\text{B } 8)$$

$$\text{Im} \Pi(q_0; q) = \frac{1}{16} \int \frac{dk}{2\pi} \frac{q_0^2 - 4E^2}{E^2 - q^2/4} D(q_0; q^2); \quad (\text{B } 9)$$

$$\Pi_{\text{m}}(q_0; q) = 2M \int \frac{d^3k}{(2\pi)^3} I_1(q_0); \quad (\text{B } 10)$$

$$\text{Im} \Pi_{\text{m}}(q_0; q) = \frac{4M}{16} \int \frac{dk}{2\pi} D_1(q_0; q^2); \quad (\text{B } 11)$$

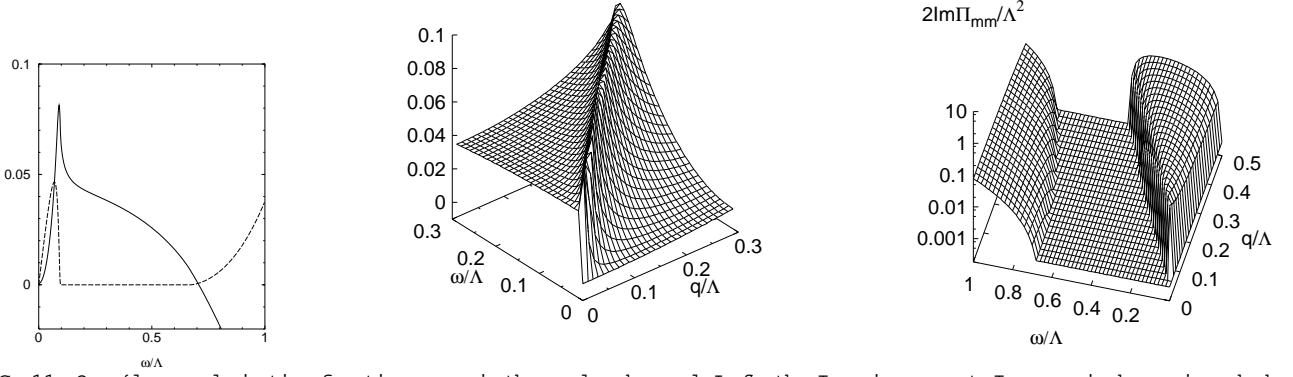


FIG. 11. One-loop polarization function Π_m in the scalar channel. Left: the imaginary part, $\text{Im } \Pi_m$ is shown in a dashed line and $\text{Re } \Pi_m$ is in a solid line. Right: the real part $\text{Re } \Pi_m$ is shown in the $(\omega/\Lambda, q/\Lambda)$ plane.

$$\begin{aligned} \Pi_m(q) = & \int \frac{d^3k}{(2\pi)^3} \frac{1}{E_1} \frac{n_{+1} - n_{-1}}{E_1^2 + k^2} \\ & + \int \frac{d^3k}{(2\pi)^3} \frac{(q_0^2 - 4E^2)(E^2 + k^2) - E^2 q^2 + (k - q)^2}{(E^2 + k^2)^2} I(q) + \frac{(q_0^2 - 4E^2)I(q)}{2} ; \end{aligned} \quad (\text{B } 12)$$

$$\text{Im } \Pi_m(q) = \frac{1}{16} \int \frac{dk}{4\pi} \frac{(q_0^2 - 4E^2)(E^2 + k^2 - q^2/4)}{E^2 + k^2} D(q; q^2) + 2 \frac{(q_0^2 - 4E^2)D(q; q^2)}{4} ; \quad (\text{B } 13)$$

$$\Pi_m(q) = M \int \frac{d^3k}{(2\pi)^3} \frac{1}{E_1} \frac{n_{+1} - n_{-1}}{E_1^2 + k^2} + M \int \frac{d^3k}{(2\pi)^3} \frac{(q_0^2 - 4E^2)I(q)}{(E^2 + k^2)^2} - 2 I(q) ; \quad (\text{B } 14)$$

$$\text{Im } \Pi_m(q) = \frac{M}{16} \int \frac{dk}{4\pi} \frac{(q_0^2 - 4E^2 + q^2/4)D(q; q^2) - 4 D(q; q^2)}{4} ; \quad (\text{B } 15)$$

$$\begin{aligned} \Pi_m(q) = & \int \frac{d^3k}{(2\pi)^3} \frac{1}{E_1} \frac{n_{+1} - n_{-1}}{E_1^2 + k^2} \\ & + \int \frac{d^3k}{(2\pi)^3} \left[\frac{(q_0^2 - 4E^2 + q^2)I(q)}{2} + \frac{1}{2} (q_0^2 - 4E^2)I(q) \right] ; \end{aligned} \quad (\text{B } 16)$$

$$\text{Im } \Pi_m(q) = \frac{1}{16} \int \frac{dk}{4\pi} \frac{(q_0^2 - 4E^2 + q^2)D(q; q^2) - (q_0^2 - 4E^2)D(q; q^2)}{4} ; \quad (\text{B } 17)$$

In these expressions we introduced a function

$$D(q; q^2) = (n_{+1} + n_{-2} - n_{-1} - n_{+2}) \quad (\text{B } 18)$$

with the sign '+' for $4M^2 < q^2 < 4(M^2 + k_{\text{max}}^2)$ and '-' for $q^2 < 0$.

It is known [?] that the response functions have a non-analytic property at the origin of the (ω, q) plane when the phonon mode spectrum exists. For demonstration we show in Fig. 11 the real and imaginary parts of $\Pi_m(\omega, q)$ with $q = 0.1$. An abrupt change of the real part is seen in the region $\omega < 0.1$, which is clearly caused by the phonon spectrum in accord with the dispersion relation. In the $q \rightarrow 0$ limit, the imaginary part becomes proportional to ω^2 , which leads to the discontinuity of the real part of Π_m as mentioned in Eq. (19) and shown in Fig. 11. In the case of the massless quarks, on the other hand, the scalar channel does not couple to the phonon motion in the $q \rightarrow 0$ limit due to the chiral symmetry. Hence the real part is non-singular at the origin as shown in Fig. 12.

In Appendix A it is shown that the spectral function for a conserved density fluctuation must be proportional to ω^2 as $q \rightarrow 0$ in general. We confirm that this requirement is fulfilled by these one-loop polarizations, Π_m , and Π_m .

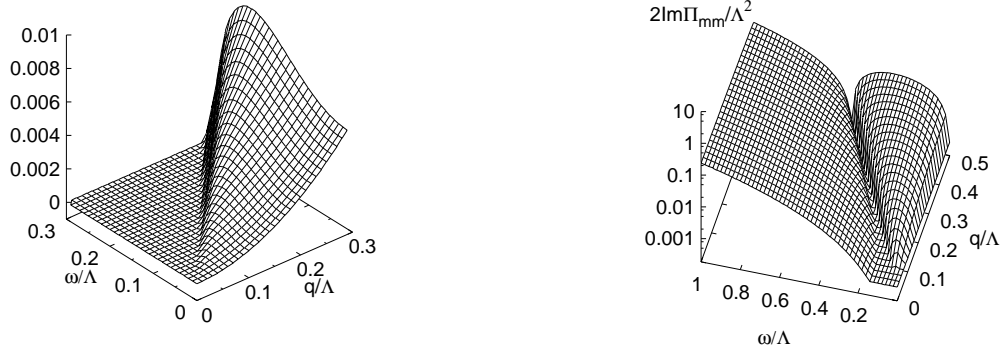


FIG. 12. One-loop polarization function in the scalar channel with massless quarks (TCP); $1/(2g)\text{Re } \Pi_{mm}$ and $\text{Im } \Pi_{mm}$.

2. susceptibilities

The susceptibilities in free quark gas with mass M are found as

$$\begin{aligned}
 \chi_{mm}^{(0)} &= \int \frac{d^3k}{(2\pi)^3} \frac{1}{E} (1 - n_+ - n_-) \frac{M^2}{E^2} \frac{1}{E} n_+ - n_- + n_+^0 + n_-^0 ; \\
 \chi_m^{(0)} &= \int \frac{d^3k}{(2\pi)^3} \frac{M}{E} (n_+^0 - n_-^0) ; \\
 \chi_{mT}^{(0)} &= \int \frac{d^3k}{(2\pi)^3} \frac{M}{E} \left(\frac{E}{T} n_+^0 + \frac{E}{T} n_-^0 \right) ; \\
 \chi^{(0)} &= \int \frac{d^3k}{(2\pi)^3} (n_+^0 + n_-^0) ; \\
 \chi_{TT}^{(0)} &= \int \frac{d^3k}{(2\pi)^3} \left(\frac{E}{T} n_+^0 + \frac{E}{T} n_-^0 \right) ; \\
 \chi_T^{(0)} &= \int \frac{d^3k}{(2\pi)^3} \left(\frac{E}{T} n_+^0 + \frac{E}{T} n_-^0 \right) ;
 \end{aligned} \tag{B 19}$$

These expressions coincide with the static one-loop polarizations in the $q \rightarrow 0$ limit. Through this limiting procedure we find that the terms containing n^0 are related with the p(h) spectrum parts in functions I and I_1 , and that all susceptibilities, except for the scalar, must accompany n^0 because of their conserved nature.

We also notice the fact of no mixing of the scalar fluctuation with others in the massless quark gas $M = 0$. In the case of $\mu = 0$, the vector fluctuation does not mix with others. Both of these originate from the symmetries. If we write down the GLE effective potential, it must be invariant under $U(1)$ and/or $U(1)$, respectively, and therefore any linear mixing with other densities is impossible.

APPENDIX C: CHIRAL QUARK MODEL

The chiral quark model may be used to perform the same analysis as in the NJL model:

$$\mathcal{L}_q = \frac{1}{2} (\partial_\mu \psi)^2 - \frac{1}{2} \bar{\psi} \not{m} \psi - \frac{1}{4!} (\bar{\psi} \psi)^2 + h \bar{\psi} \psi + g (\bar{\psi} \psi) (\psi^\dagger \psi) ; \tag{C 1}$$

where $\psi = \psi_a$, $\psi_a = \psi_a$, and $\bar{\psi} \psi < 0$. The meson mode is introduced as an elementary field with the kinetic term here.

Within the mean field approximation for ψ and $\bar{\psi}$, we obtain the effective potential after integrating out the quark field as

$$q(T; \mu; \beta) = V = - \ln Z = - \ln \int d\psi d\bar{\psi} \exp \left[- \int d^4x \left(\bar{\psi} (i \not{D} - m) \psi + \frac{1}{2} (\sigma^2 + \frac{1}{4!} (\sigma^4)^2) \right) \right] \frac{d^3k}{(2\pi)^3} \exp \left[- T \ln(1 - n_+) - T \ln(1 - n_-) \right] \quad (C2)$$

with $E = \sqrt{M^2 + k^2}$ and $M = g$. The divergent vacuum contribution of the quark fluctuation appears as the first term in the integrand in Eq. (C2), and requires a regularization/renormalization. As a simplest prescription we usually assume that the renormalization is already done in the vacuum, and discard this term. Then the parameters are fixed so as to reproduce the pion decay constant, the pion and sigma masses, and the constituent quark mass in the vacuum, as in Ref. [16]. We find the Z_2 CP at $(T_c; \mu_c) = (117.7, 176.2)$ MeV.

Within the same level of the approximation we calculate the scalar response function, obtaining

$$\chi = \frac{1}{q^2 + m^2 + \frac{1}{2} \frac{g^2}{m m}}; \quad (C3)$$

where the polarization χ_{mm} is defined in Eq.(26) with $\mu = 1$, but whose vacuum part is removed, that is, the term $1 - n_+ - n_-$ is replaced with $n_+ - n_-$ (see Appendix B). Other response functions have the same structure with the NJL result (25) at RPA level because we assume the same scalar interaction between quarks. We find the same spectral enhancement in the space-like momentum region at Z_2 CP as in the NJL model, and the ratio R defined (31) shows the similar behavior.

We should note, however, that the spectral function of the scalar channel does not satisfy the semi-positivity condition in the time-like momentum region in this treatment. This happens because our simple regularization breaks the detailed balance relation which is essential to assure thermal equilibrium. Hence the result of the spectrum in this chiral quark model should be interpreted with caution, especially in the time-like region. This defect may be related with the fact that the effective potential (C2) with the vacuum contribution subtracted does not have an analytic expansion in terms of μ around $\mu = 0$ due to an infrared divergence. Because of this difficulty, we could not find the TCP in the chiral quark model with the regularization adopted here.

- [1] B. Svetitsky and L.G. Ya e, Nucl. Phys. B 210, 423 (1982).
- [2] R.D. Pisarski and F.W. Ilczek, Phys. Rev. D 29, 338 (1984).
- [3] For review, e.g., Quark-Gluon Plasma 3, eds. R.C. Hwa and X.N. Wang, World Scientific Singapore, to be published.
- [4] M.A. Stephanov, K. Rajagopal and E.V. Shuryak, Phys. Rev. Lett. 81 4816 (1998).
- [5] M.A. Stephanov, K. Rajagopal and E.V. Shuryak, Phys. Rev. D 60 114028 (1999).
- [6] For review, e.g., M.A. Stephanov, to appear in Prog. Theor. Phys. Suppl. [arXiv:hep-ph/0402115].
- [7] M. Asakawa and K. Yazaki, Nucl. Phys. A 504 668 (1989).
- [8] S. Gavin, A. Gocksch, R.D. Pisarski, Phys. Rev. D 49 3079 (1994).
- [9] J. Berges and K. Rajagopal, Nucl. Phys. B 538 215 (1999).
- [10] M.A. Halasz, A.D. Jackson, R.E. Shrock, M.A. Stephanov, and J.J.M. Verbaarschot, Phys. Rev. D 58 096007 (1998).
- [11] Z. Fodor and S.D. Katz, JHEP 0203, 014 (2002).
- [12] P. de Forcrand and O. Philipsen, arXiv:hep-lat/0309109.
- [13] F. Karsch, C.R. Allton, S. Ejiri, S.J. Hands, O. Kaczmarek, E. Laermann and C. Schmidt, arXiv:hep-lat/0309116.
- [14] B. Bercdnikov and K. Rajagopal, Phys. Rev. D 61 105017, (2000).
- [15] Y. Hatta and T. Ikeda, Phys. Rev. D 67 014028 (2003).
- [16] O. Scavenius, A. Mocsy, I.N. Mishustin and D.H. Rischke, Phys. Rev. C 64 045202 (2001).
- [17] S. Borsanyi, A. Patkos, D. Sexty, Z. Szep, Phys. Rev. D 64 125011 (2001).
- [18] Y. Hatta and M.A. Stephanov, Phys. Rev. Lett. 91 102003, 2003, Erratum -ibid, 129901 (2003).
- [19] F. Karsch, E. Laermann and C. Schmidt, Phys. Lett. B 520, 41 (2001).
- [20] H. Fujii, Phys. Rev. D 67 094018 (2003).
- [21] H. Fujii and M. Ohtani, to appear in Prog. Theor. Phys. Suppl. [arXiv:hep-ph/0401028].
- [22] D. Forster, Hydrodynamic Fluctuations, Broken Symmetry, and Correlation Functions (W. A. Benjamin, Inc., Massachusetts, 1975).
- [23] T. Hatsuda and T. Kunihiro, Phys. Rept. 247 221 (1994).
- [24] P. Chakraborty, M.G. Mustafa, M.H. Thoma, Phys. Rev. D 68 085012 (2003).
- [25] I. Lawrie and S. Sarbach, in Phase Transitions and Critical Phenomena, ed. by C. Domb and J. Lebowitz (Academic Press, NY, 1984), Vol. 9, pp. 1.
- [26] P.C. Hohenberg and B.I. Halperin, Rev. Mod. Phys. 49 435 (1977).
- [27] D.T. Son and M.A. Stephanov, arXiv:hep-ph/0401052.

- [28] Y. Nambu and G. Jona-Lasinio, Phys. Rev. 122 345 (1961); 124 246 (1961).
- [29] S. P. Klevansky Rev. Mod. Phys. 64 649 (1992).
- [30] M. Le Bellac, Thermal Field Theory, (Cambridge University Press, Cambridge, England, 1996).
- [31] T. Hatsuda and T. Kunihiro, Phys. Rev. Lett. 55 158 (1985).
- [32] C. Schmidt, C. R. Allton, S. Ejiri, S. J. Hands, O. Kaczmarek, F. Karsch and E. Laermann, Nucl. Phys. Proc. Suppl. 119, 517 (2003).
- [33] D. T. Son and M. A. Stephanov, Phys. Rev. Lett. 86, 592 (2001).
- [34] For review, e.g., S. Y. Jeon and V. Koch, arXiv:hep-ph/0304012.